Clays and Clay Minerals, Vol. 35, No. 2, 129–138, 1987.

REFINEMENT OF THE CRYSTAL STRUCTURE OF A MONOCLINIC FERROAN CLINOCHLORE

AUDREY C. RULE AND S. W. BAILEY

Department of Geology & Geophysics, University of Wisconsin
Madison, Wisconsin 53706

Abstract—A monoclinic II*b*-2 clinochlore from Washington, D.C., contrary to previous studies, is primarily a ferroan rather than a ferrian chlorite. Disorder of tetrahedral Si,Al cations is indicated because of unsuccessful structural refinements in subgroup symmetries. The true space group is $C2/m$. Slight ordering of Mg, Fe^{2+}, and Fe^{3+} over octahedra M(1) and M(2) within the 2:1 layer (mean M–O,OH = 2.092 and 2.084 Å, respectively), complete ordering of trivalent Al into the centrosymmetric octahedron M(4) of the interlayer sheet (M–OH = 1.929 Å), and ordering of primarily divalent cations (Mg and Fe) into the two interlayer M(3) octahedra (M–OH = 2.117 Å) exist. The excess of negative charge above unity due to tetrahedral substitution of Al for Si (1.378 atoms) is compensated entirely within the octahedral sheet of the 2:1 layer.

Ordering of a trivalent cation into one octahedron in the interlayer should be universal for all stable trioctahedral chlorites. In this specimen the ordering is due to (1) minimization of cation-cation repulsion by layer offsets which provide more space around the trivalent element, and (2) energy minimization by localization of the source of positive charge on the interlayer sheet in one octahedron rather than two. In other structures or for different compositions additional factors can be important also. Most chlorites of the II*b* and *Ib* ($\beta = 90°$) types are expected to show disorder of the tetrahedral cations. The *b* positioning of interlayer and layer provides no preferential driving force for concentration of Si and Al in any tetrahedron as a consequence of the expected ordering of the interlayer cations. The monoclinic II*b*-2 polytype is less abundant in nature than the triclinic II*b*-4 and II*b*-6 structures, because only half as many possible superpositions of layers exist that will produce monoclinic symmetry. Crystallization factors must also be important, because the II*b*-2 chlorite is much less abundant than predicted by this purely geometrical argument.

Key Words—Charge balance, Chlorite, Clinochlore, Crystal structure, Order-disorder.

INTRODUCTION

Only two studies (Steinfink, 1958, 1961; Brown and Bailey, 1963) involving structural refinements of trioctahedral chlorite species have reported ordering of tetrahedral Si,Al cations. Both refinements were based on film data and, because of the limited computer facilities available at the time, achieved only a moderate degree of refinement. One of these studies was of a chromian clinochlore from Erzincan, Turkey, having the I*a*-4 stacking arrangement. Ordering of both tetrahedral and interlayer cations was reported (Brown and Bailey, 1963). Subsequent refinement of this chromian clinochlore, using the same crystal as the earlier study, confirmed the ordering of the interlayer cations, but found complete disorder of the tetrahedral cations (Bailey, 1986). The present study re-examines the second trioctahedral chlorite for which ordering of tetrahedral cations was claimed.

Steinfink (1958, 1961) reported ordering of tetrahedral, 2:1 layer octahedral, and interlayer octahedral cations in a ferroan clinochlore (labeled prochlorite) from a waterworks tunnel excavation in Washington, D.C. An interesting point about the chemistry of this specimen is that an old chemical analysis (Clarke and Schneider, 1891) reported 17.77% FeO and 2.86% Fe_2O_3, but a later analysis by the Shell Research Laboratory (Steinfink, 1958) indicated a complete reversal of the valencies, that is 2.7% FeO and 20.0% Fe_2O_3. Steinfink believed the specimen had oxidized at some time after its original collection and used the ferric composition for discussion of its structure and crystal chemistry. A Mössbauer analysis of the specimen by Lisa Heller-Kallai (Department of Geology, Hebrew University, Jerusalem, personal communications, 1982 and 1985), however, found the iron to be predominantly ferrous. A microprobe analysis of the sample by Bailey (1972) indicated oxide totals close to those of the 1891 analysis, and the Fe^{2+}/Fe^{3+} ratio is taken in this paper to be the 6.9 value determined in the latter analysis.

The structural type of this chlorite also makes the sample of special interest because it is a regularly stacked, one-layer II*b*-2 polytype having monoclinic symmetry. The ideal space group of $C2/m$ for this polytype was reported by Steinfink (1958) to be lowered to $C2$ symmetry as a consequence of the cation ordering. The II*b* arrangement of layers and interlayers is the most abundant and most stable form of trioctahedral chlorite, estimated to represent about 80% of all natural specimens (Bailey and Brown, 1962), but

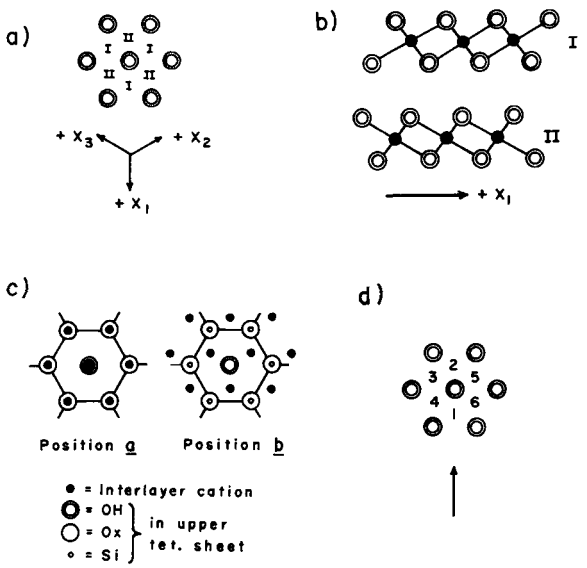

Figure 1. (a) Definition of I and II sets of octahedral cation positions above OH plane in the interlayer sheet relative to a *fixed* set of hexagonal axes. (b) Interlayer sheet slants in opposite directions for cations occupying the I and II positions. (c) Superposition patterns *a* and *b* of interlayer cations relative to a hexagonal ring in adjacent 2:1 layer. (d) Six positions providing interlayer hydrogen bonds if center of a hexagonal ring at base of repeating 2:1 layer is placed over one of the numbers. Double circles are OH groups in upper anion plane of interlayer sheet, and arrow is the direction of *a*/3 shift within the first 2:1 layer and lies on the symmetry plane of that layer.

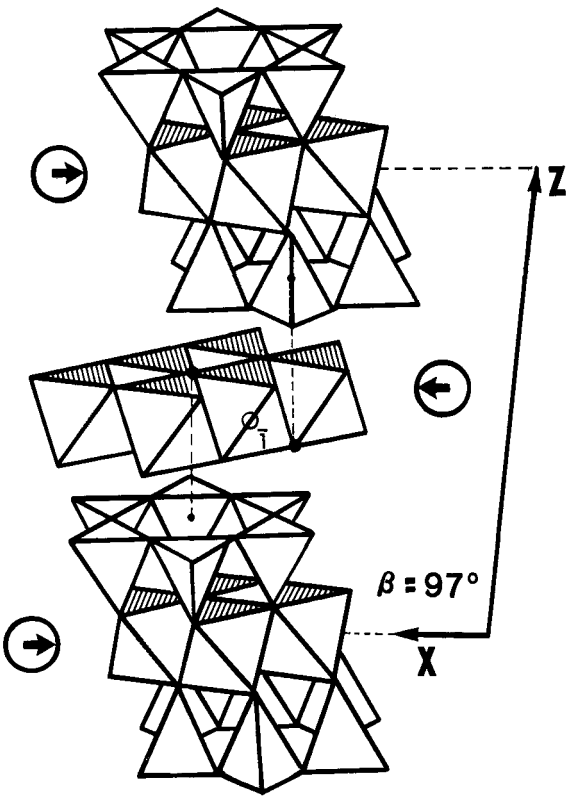

Figure 2. [010] diagrammatic view of II*b*-2 structure. Arrows within circles indicate slant directions of octahedral sheets. Interlayer sheet has opposite slant to that of the octahedral sheet in the 2:1 layer for II type chlorite. Vertical dashed lines show alignment of an OH group in interlayer with the centers of 6-fold rings of the tetrahedral sheets below and above found in the *b* relative position of interlayer to 2:1 layers. Alignment differs for *a* relative positions.

most specimens are of the triclinic polytype II*b*-4 (=II*b*-6). All recent structural refinements of the triclinic II*b*-4 form have found complete disorder of tetrahedral Si,Al cations (Phillips *et al.,* 1980; Joswig *et al.,* 1980), and Phillips *et al.* (1980) suggested that this disorder gives the most favorable balance of charge around the site of the ordered R^{3+} cation present in the interlayer sheet. The monoclinic II*b*-2 polytype is rare, but the relationship of its reported ordering to its stability is of considerable interest. The original refinement was of only moderate accuracy, as indicated by its residual of R = 13.1%, and further refinement of the structure is warranted.

A portion of the same sample used by Steinfink was obtained from the U.S. National Museum (sample #45875) for the purpose of a new structural refinement. The goals of the present study were: (1) to determine the degree of cation ordering by a refinement of greater accuracy, (2) to relate any ordering found to the local charge balance and stability of the monoclinic II*b*-2 polytype, (3) to determine the hydrogen bonding system by location of the H^+ protons of the OH groups, and (4) to determine the reason for the scarcity of the II*b*-2 structure in nature.

THE II*b*-2 CHLORITE POLYTYPE

The II*b*-2 structure is one of 12 possible ideal one-layer chlorite polytypes derived by Bailey and Brown (1962). Its symbol in the terminology of Lister and Bailey (1967) is $-x_1$-II*b*-2. In one-layer chlorites the orientation and the position of the interlayer sheet relative to the 2:1 layers below and above are the only variables in the structure; they are specified in the structural symbol. In the II*b*-2 symbol, the II means that the orientation of the interlayer sheet is such that its slant is opposite in direction to that of the octahedral sheet in the initial 2:1 layer (Figures 1a and 1b; Figure 2). Next, the interlayer sheet is located in the *b* position (Figure 1c) above the initial 2:1 layer so that long hydrogen bonds form between adjacent oxygen and hydroxyl surfaces. This *b* position of the interlayer does not superimpose cations and is inherently more stable than the alternative *a* position, in which direct superposition of interlayer cations on tetrahedral cations causes cation-cation repulsion.

https://doi.org/10.1346/CCMN.1987.0350205 Published online by Cambridge University Press

Table 1. Chemical composition.

Oxide	Wt. %	Atoms	
SiO_2	25.50	2.622	4.000
Al_2O_3	22.23	1.378	
		1.316	
MgO	18.58	2.847	5.920
FeO	17.83	1.533	
Fe_2O_3	2.87	0.222	
Cr_2O_3	0.03	0.002	

Analysis by ARL EMX microprobe. Each value is an average of measurements on five grains. A 15-kV, 0.02-μA beam was used and focused at 10 μm to avoid specimen damage. Standards: wollastonite (Si), hematite (Fe), MgO (Mg), corundum (Al), and chromian chlorite (Cr). Corrections were made by the ZAF method. Allocation to a structural formula assumed 28 positive charges and the Fe^{2+}/Fe^{3+} ratio of 6.9 determined by Clarke and Schneider (1891). M. Brauner, analyst.

The final consideration in describing the polytype is articulation of the repeating 2:1 layer with the top of the interlayer sheet. Six positions exist that yield optimum hydrogen bonding between adjacent surfaces. These positions are numbered according to the position that the center of a tetrahedral ring in the repeating 2:1 layer can take in projection onto the upper plane of hydroxyls of the interlayer sheet (Figure 1d). In the II*b*-2 structure, the repeating 2:1 layer is positioned such the center of a hexagonal ring of basal oxygens projects onto position 2. This position, along with positions 4 and 6 (all of the even numbers), produces *b*-type relative arrangements of the interlayer and the repeating 2:1 layer, i.e., the interlayer sheet is then symmetric in that it has *b* positions relative to the 2:1 layers both below and above (Figure 2). Because position 2 lies on the mirror plane of the initial part of the structure, the mirror relationship holds for the entire structure. The resulting symmetry is monoclinic *C*2/*m*. Positions 4 and 6 do not fall on the initial mirror plane and thus produce resultant triclinic polytypes of ideal symmetry $C\bar{1}$. The center of an hexagonal ring in position 2 is offset by $a_1/3$ across the interlayer relative to an hexagonal ring at the top of the 2:1 layer below, i.e., the rings do not oppose each other as they do in micas. To retain the standard β angle of 97°, the $+X_1$ direction in Figure 2 has been reversed relative to the fixed initial direction used in Figure 1 to define I and II octahedral sites. This configuration gives a resultant offset of $a/3$ for the repeating layer, rather than $2a/3$.

EXPERIMENTAL

A bright green crystal (University of Wisconsin Geology Museum #1769/6), about 0.24 × 0.20 × 0.05 mm in size, from the waterworks tunnel specimen was chosen for study because of its sharp extinction under the polarizing microscope. All X-ray diffraction spots on Weissenberg photographs of this crystal, as well as all other crystals examined, showed some streaking due to a visible curved growth of the crystal. The *hkl* diffraction spots with $k \neq 3n$ were as sharp as *hkl* spots with $k = 3n$, however, indicating that the stacking arrangement was well ordered. True *X* and *Y* directions determined from Weissenberg photographs were parallel to the optical extinction directions on (001). The chemical composition (Table 1) as determined by electron microprobe analysis and assuming Fe^{2+}/Fe^{3+} of 6.9 and 28 positive charges is $(Mg_{2.847}Fe^{2+}_{1.533}Fe^{3+}_{0.222}Al_{1.316}Cr_{0.002}\square_{0.080})(Si_{2.622}Al_{1.378})O_{10}(OH)_8$.

Unit-cell parameters of $a = 5.350(3)$, $b = 9.267(5)$, $c = 14.27(1)$ Å, and $\beta = 96.35(5)°$ were determined by least-squares refinement of 15 low- to medium-angle reflections. Intensities of 4447 reflections were collected over all octants as far as $2\theta = 60°$ with a Nicolet $P2_1$ automated single-crystal diffractometer in the θ:2θ variable-scan mode using graphite monochromated MoKα radiation. These reflections were merged into 767 independent, monoclinic, non-zero reflections. Crystal and electronic stability were checked after every 25 reflections by monitoring one standard reflection. The integrated intensity (I) was calculated from I = [S − (B1 + B2)/Br]Tr, where S is the scan count, B1 and B2 the background counts, Br is the ratio of background time to scan time, and Tr is the 2θ scan rate in °/min. Reflections were considered to be observed if $I > 2\sigma(I)$. Integrated intensities were corrected for Lp factors and for absorption by using the semi-empirical psi-scan technique of North *et al.* (1968).

REFINEMENT IN IDEAL SPACE GROUP *C*2/*m*

Atomic positions for the monoclinic II*b*-2 chlorite stacking arrangement on the basis of undistorted sheets (Bailey and Brown, 1962) were used as the starting point for refinement in ideal space group *C*2/*m*, assuming complete cation disorder and using a modified least-squares program ORFLS (Busing *et al.*, 1962). Scattering factors from Cromer and Mann (1968) corresponding to 50% ionization were used in the refinement. Space group *C*2/*m* requires that all tetrahedral positions be equivalent, and the centers of symmetry allow only two unique octahedra in each of the octahedral sheets.

A few cycles of refinement indicated that unit weights were more appropriate to the data than sigma weights, and these were used for the balance of the refinement. After five cycles of refinement (residual unweighted R = 17.0%) a difference-electron density map (DED map) was made which showed a small amount of ordering between M(1) and M(2) in the 2:1 layer octahedral sites and a larger difference of about six electrons between the M(3) and M(4) interlayer octahedral sites. Scattering factor tables were revised accordingly, and one more cycle of refinement brought R to 16.5%. Both

Table 2. Final atomic positions and thermal parameters.

	x/a	y/b	z/c	B(equiv)	β(1,1)	β(2,2)	β(3,3)	β(1,2)	β(1,3)	β(2,3)
M(1)	0	0	0	1.25	0.0038(13)	0.0026(5)	0.0030(3)	0	0.0009(5)	0
M(2)	0	0.3322(4)	0	1.36	0.0051(9)	0.0029(3)	0.0031(8)	0	0.0010(3)	0
OH(1)	0.185(2)	0.5	0.0743(9)	1.91	0.0098(33)	0.0057(13)	0.0033(6)	0	0.0013(11)	0
O(1)	0.189(1)	0.1667(9)	0.0774(6)	1.85	0.0093(20)	0.0044(8)	0.0037(4)	0.0004(13)	0.0010(7)	0.0000(5)
T(1)	0.2248(5)	0.1669(3)	0.1937(2)	1.41	0.0058(7)	0.0034(3)	0.0030(1)	0.0001(5)	0.0005(2)	−0.0001(2)
O(2)	0.197(2)	0	0.2357(9)	2.18	0.0125(35)	0.0046(12)	0.0044(7)	0	0.0016(12)	0
O(3)	0.511(1)	0.2280(10)	0.2363(6)	2.35	0.0088(22)	0.0061(10)	0.0049(5)	−0.0006(12)	0.0013(8)	0
OH(2)	0.172(2)	0	0.4289(8)	1.58	0.0071(30)	0.0042(12)	0.0031(6)	0	0.0001(10)	0
OH(3)	0.131(1)	0.3463(8)	0.4285(5)	1.63	0.0067(19)	0.0045(9)	0.0032(4)	0.0002(11)	0.0009(7)	−0.0004(5)
M(3)	0	0.1664(4)	0.5	1.45	0.0035(9)	0.0033(3)	0.0035(2)	0	0.007(3)	0
M(4)	0	0.5	0.5	1.33	0.0039(17)	0.0033(7)	0.0030(4)	0	0.0006(6)	0
H(1)	0.2113	0.5	0.1448							
H(2)	0.1623	0	0.3661							
H(3)	0.1586	0.3359	0.3698							

Errors in parentheses are for last decimal place listed. H(1), H(2), and H(3) were assigned isotropic temperature factors of 2.0. B(equiv) = 4/3[β(1,1)/(a*)² + β(2,2)/(b*)² + β(3,3)/(c*)²].

Table 3. Shape and orientation of thermal ellipsoids.

Atom	Axis	RMS displacement (Å)	Angle (°) with respect to X	Y	Z
M(1)	r1	0.072(13)	180(4)	90	84(4)
	r2	0.107(10)	90	0	90
	r3	0.175(8)	90(4)	90	174(4)
M(2)	r1	0.083(7)	180(3)	90	83(3)
	r2	0.113(6)	90	0	90
	r3	0.178(5)	90(3)	90	173(3)
OH(1)	r1	0.117(20)	177(12)	90	81(12)
	r2	0.158(18)	90	0	90
	r3	0.184(17)	93(12)	90	171(12)
O(1)	r1	0.114(13)	171(28)	81(28)	84(6)
	r2	0.139(13)	81(28)	9(28)	91(11)
	r3	0.193(11)	90(7)	90(11)	174(6)
T(1)	r1	0.091(6)	175(7)	87(11)	88(2)
	r2	0.122(5)	87(11)	4(10)	89(5)
	r3	0.174(4)	86(3)	88(5)	177(3)
O(2)	r1	0.131(19)	177(10)	90	81(10)
	r2	0.141(19)	90	0	90
	r3	0.211(17)	93(10)	90	171(10)
O(3)	r1	0.110(14)	174(12)	96(12)	84(5)
	r2	0.163(13)	96(12)	7(12)	92(9)
	r3	0.224(12)	89(5)	93(9)	174(6)
OH(2)	r1	0.101(21)	172(10)	90	92(10)
	r2	0.135(19)	90	0	90
	r3	0.180(17)	82(10)	90	178(10)
OH(3)	r1	0.097(14)	176(16)	86(16)	84(7)
	r2	0.138(13)	86(16)	13(13)	79(12)
	r3	0.184(11)	89(6)	78(12)	167(11)
M(3)	r1	0.070(9)	177(2)	90	86(2)
	r2	0.119(6)	90	0	90
	r3	0.189(5)	87(2)	90	176(2)
M(4)	r1	0.075(17)	177(5)	90	87(5)
	r2	0.120(12)	90	0	90
	r3	0.175(10)	87(5)	90	177(5)

positional parameters and isotropic temperature factors were varied next to bring R to 12.6%. Another DED map suggested further changes in octahedral cation scattering factors, including only a four electron difference between M(3) and M(4). Continued refinement with anisotropic temperature factors produced an R of 7.8%. At this point the hydrogen protons of the OH groups were located on another DED map as volumes of excess electron density (about 0.65 e^- each). Further least-squares refinement with the hydrogens added (but not varied) produced a final unweighted residual of 7.6%. Fortran programs SHELLS (W. A. Dollase, Department of Geology, University of California at Los Angeles, Los Angeles, California, unpublished) and ORFFE (Busing *et al.,* 1964) were used for determination of structural bond lengths and errors. Final atomic and thermal parameters are listed in Table 2. The shape and orientation of the thermal ellipsoids are presented in Table 3 and bond lengths and

Table 4. Interatomic distances and angles.

T(1)–O bond lengths (Å)		T(1) edge lengths (Å)		T(1) bond angles (°)	
T(1)–O(1)	1.649(9)	O(1)–O(2)	2.734(13)	O(1)–T(1)–O(2)	110.8(5)
T(1)–O(2)	1.672(6)	O(1)–O(3)	2.735(12)	O(1)–T(1)–O(3)	111.4(4)
T(1)–O(3)	1.681(8)	O(1)–O(3)	2.752(12)	O(1)–T(1)–O(3)	111.1(4)
T(1)–O(3)	1.669(8)	O(2)–O(3)	2.697(10)	O(2)–T(1)–O(3)	108.5(5)
mean	1.668(4)	O(2)–O(3)	2.712(10)	O(2)–T(1)–O(3)	107.1(5)
		O(3)–O(3)	2.706(3)	O(3)–T(1)–O(3)	107.8(3)
		mean	2.723(4)	mean	109.4(2)

2:1 layer				Interlayer			
M(1)–O,OH bond lengths (Å)		M(2)–O,OH bond lengths (Å)		M(3)–OH bond lengths (Å)		M(4)–OH bond lengths (Å)	
M(1)–OH(1)	2.089(11) × 2	M(2)–OH(1)	2.070(8) × 2	M(3)–OH(2)	2.113(8) × 2	M(4)–OH(2)	1.926(10) × 2
M(1)–O(1)	2.093(8) × 4	M(2)–O(1)	2.085(8) × 2	M(3)–OH(3)	2.122(7) × 2	M(4)–OH(3)	1.930(7) × 4
mean	2.092(4)	M(2)–O(1)	2.097(7) × 2	M(3)–OH(3)	2.115(8) × 2	mean	1.929(3)
		mean	2.084(3)	mean	2.117(3)		
M(1) shared diagonal edges (Å)		M(2) shared diagonal edges (Å)		M(3) shared diagonal edges (Å)		M(4) shared diagonal edges (Å)	
OH(1)–O(1)	2.802(11) × 4	OH(1)–OH(1)	2.732(23)	OH(2)–OH(2)	2.889(21)	OH(2)–OH(3)	2.609(11) × 4
O(1)–O(1)	2.823(15) × 2	O(1)–O(1)	2.823(15)	OH(2)–OH(3)	2.609(11) × 2	OH(3)–OH(3)	2.603(14) × 2
mean	2.809(5)	OH(1)–O(1)	2.802(11) × 2	OH(3)–OH(3)	2.897(15) × 2	mean	2.607(5)
		O(1)–O(1)	2.830(16) × 2	OH(3)–OH(3)	2.603(14)		
		mean	2.803(6)	mean	2.751(6)		
M(1) unshared lateral edges (Å)		M(2) unshared lateral edges (Å)		M(3) unshared lateral edges (Å)		M(4) unshared lateral edges (Å)	
OH(1)–O(1)	3.105(13) × 4	O(1)–OH(1)	3.089(8) × 2	OH(2)–OH(3)	3.217(8) × 2	OH(2)–OH(3)	2.840(11) × 4
O(1)–O(1)	3.090(16) × 2	O(1)–O(1)	3.088(8) × 2	OH(2)–OH(3)	3.225(11) × 2	OH(3)–OH(3)	2.849(15) × 2
mean	3.100(6)	O(1)–OH(1)	3.074(13) × 2	OH(3)–OH(3)	3.216(9) × 2	mean	2.843(5)
		mean	3.084(4)	mean	3.219(4)		

$OH–H^+$ distances (Å)		OH–O distances (Å)		Basal oxygen-H^+ distances (Å)		Basal oxygen-interlayer hydroxyl separation (Å)
OH(1)–H(1)	1.001(12)	O(2)–OH(2)	2.774(17)	O(2)–H(2)	1.890(12)	2.731
OH(2)–H(2)	0.892(11)	O(3)–OH(3)	2.831(12) × 2	O(3)–H(3)	2.066(9) × 2	
OH(3)–H(3)	0.871(7) × 2					

Hydrogen bond angles (°)		2:1 layer hydrogen ρ (°)
OH(2)–H(2)–O(2)	171.3(7)	ρ = 88.2
OH(3)–H(3)–O(3)	146.1(5) × 2	

Table 5. Summary of octahedral and tetrahedral parameters.

	2:1 layer octahedra		Interlayer octahedra	
	M(1)	M(2)	M(3)	M(4)
Composition	0.50 Mg 0.39 Fe^{2+} 0.07 Al 0.04 □	0.59 Mg 0.26 Fe^{2+} 0.08 Al 0.068 Fe^{3+} 0.002 Cr	0.64 Mg 0.32 Fe^{2+} 0.04 Al	0.965 Al 0.035 □
Mean M–O,OH bond length (Å)	2.092(4)	2.084(3)	2.113(3)	1.929(3)
Calculated M–O,OH (Å)	2.091	2.079	2.089	1.921
Electron density observed	15.0	14.8	14.7	11.1
Electron density calculated	15.3	14.9	14.9	11.1
Octahedral sheet thickness (Å)	2.166		2.024	
Octahedral flattening (°)	58.84	58.71	61.43	58.33
Octahedral rotation (°)	0.00	0.32	7.60	0.00
RMS deviation 15 internal octahedral angles from ideal (°)	5.04	4.95	9.13	4.44
RMS deviation 36 external octahedral angles from ideal (°)	3.43	3.43	6.37	3.04
Tetrahedral sheet thickness (Å)	2.265			
Tetrahedral rotation angle α (°)	8.5			
Tetrahedral angle τ (°)	111.1			
Basal oxygen corrugation Δz (Å)	0.01			

angles in Table 4. Observed and calculated structure factors may be obtained from the authors upon request.

SUBGROUP SYMMETRIES

Space groups $C2$, Cm, $C1$, and $C\bar{1}$ are all possible subgroup symmetries of the ideal space group $C2/m$. Primitive space groups are not considered because there are no violations of C-face centering observed on films. Refinements in the two triclinic space groups, $C1$ and $C\bar{1}$, were not attempted because the data had no triclinic characteristics [i.e., $F(hkl) = F(h\bar{k}l)$ within error for all but five sets of reflections]. In addition, a triclinic DED map was prepared using the final atomic positions from refinement in space group $C2/m$, but with the data merged according to triclinic symmetry. No significant cation ordering or violations of monoclinic symmetry were detected.

Of the two monoclinic subgroups, $C2$ and Cm, space group $C2$ is more likely and is the one reported by Steinfink (1958). For completeness, however, refinements were attempted in both space groups $C2$ and Cm. Both subgroups are acentric, and two different but enantiomorphic tetrahedral cation ordering models are possible in each.

Refinement in space group C2

Three different refinements in space group $C2$ were attempted. The first two trials had starting atomic positions obtained from the distance-least-squares (DLS) program OPTDIS (Dollase, 1980). Final atomic positions from refinement in the ideal space group were used as input into this modeling program. The two tetrahedral sites were modeled so that T(1) was large and Al-rich and T(2) was small and Si-rich in the first trial and reversed for the second trial. Other atomic positions were modified slightly to avoid pseudosymmetry. In least-squares refinements of both models, the tetrahedral sites returned to their disordered arrangements with final residuals of 12.7% with isotropic temperature factors (anisotropic refinements were attempted but these failed). DED maps were prepared, but no cation ordering in addition to that identified in the ideal space group was found. All final refined atomic positions were the same within experimental error as those refined in the ideal space group. The third attempt at refinement in space group $C2$ used Steinfink's final atomic coordinates as a starting point. But after a few cycles of refinement it became clear that all atomic positions were oscillating along Y, and the refinement was stopped with R = 15%. The final atomic positions approached disorder, confirming the fact that $C2$ is not the correct space group.

Refinement in space group Cm

DLS program OPTDIS was also used to model the atomic positions for refinement in subgroup Cm. Only one of the two enantiomorphic models was refined because, in the absence of anomalous scattering, both would yield the same result. After six cycles of refinement the atoms returned to their disordered positions, with R = 12.7%. Therefore, this space group is also incorrect.

Correct space group

We conclude that the ideal space group of $C2/m$ is the correct symmetry for this chlorite. Refinement in both $C2$ and Cm subgroup symmetries resulted in the atoms returning to the disordered arrangement. Tri-

https://doi.org/10.1346/CCMN.1987.0350205 Published online by Cambridge University Press

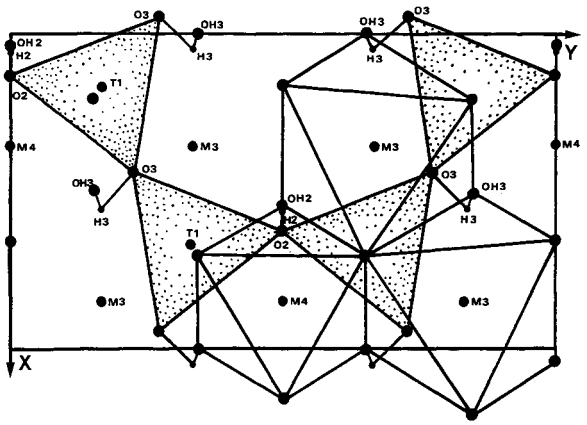

Figure 3. Interlayer octahedra in projection onto tetrahedral sheet (stippled) of lower 2:1 layer. Note distortion of large octahedron M(3) and kink in hydrogen bond OH3–H3–O3.

clinic refinements were not attempted because the data were monoclinic. The final R value for the ideal space group, 7.6%, is higher than one would expect for the correct space group, but this can be attributed to the poor crystal quality resulting from curved crystal growth.

DISCUSSION

Octahedra

Table 5 lists the observed octahedral bond lengths, octahedral compositions (as inferred from consideration of the observed M–O,OH and M–OH bond lengths, observed electron densities, and bulk compositions), calculated octahedral bond lengths and electron densities, and calculated octahedral distortions. The empirical mean bond lengths found by Weiss *et al.* (1985) for octahedral Mg, Al, Fe^{2+}, Fe^{3+}, and vacancy in micas were used to calculate bond lengths expected for the inferred compositions.

The *trans* octahedron M(1) and the two *cis* octahedra M(2) in the 2:1 layer are similar in size and amount of distortion (Table 5). M(2) is slightly smaller than M(1) because all the ferric iron is concentrated there. All the Fe in M(1) is ferrous. The negative charge on the tetrahedral sheets due to substitution of Al for Si is 1.378, and the excess of this charge above unity is compensated within the octahedral sheet of the 2:1 layer.

Octahedron M(4) on a symmetry center in the interlayer sheet is considerably smaller than M(3) and contains only Al (Table 5). Similar ordering of a trivalent element into the centrosymmetric octahedron in the interlayer sheet has been found in all trioctahedral chlorites studied in detail (Phillips *et al.*, 1980; Joswig *et al.*, 1980; Bailey, 1986). Bish and Giese (1981) determined on the basis of electrostatic energy calculations that concentration of a trivalent ion in interlayer site M(4) increases the stability of the II*b*-4 structure; such a relationship is likely for the II*b*-2 structure as well. Due to the difference in size between the M(3) and M(4) octahedra, M(3) is distorted considerably (Table 5 and Figure 3) because it must share opposite diagonal edges with a small M(4) on one side and a large M(3) on the other side. The interlayer sheet is thinner (2.024 Å) than the octahedral sheet within the 2:1 layer (2.166 Å) because of the concentration of smaller trivalent elements in the interlayer.

The agreement between observed and calculated octahedral bond lengths and electron densities in Table 5 is very good. Although Fe^{2+}, Fe^{3+}, Mg, Al, and vacancies may be distributed in many ways over the six available octahedral sites, the observed bond lengths and electron densities set definite constraints on the distribution. The total of the assigned octahedral compositions is $(Mg_{2.96}Fe^{2+}_{1.55}Fe^{3+}_{0.14}Al_{1.28}Cr_{0.002}\square_{0.075})$ relative to the analyzed composition of $(Mg_{2.85}Fe^{2+}_{1.53}Fe^{3+}_{0.22}Al_{1.32}Cr_{0.002}\square_{0.08})$.

The Mössbauer pattern is best interpreted as one major octahedral Fe^{2+} doublet and one minor octahedral Fe^{3+} doublet (Lisa Heller-Kallai, Department of Geology, Hebrew University, Jerusalem, personal communication, 1985). All the Fe^{3+} has been placed in octahedron M(2) in accord with the single local environment indicated by the Mössbauer spectra; but all the Fe^{2+} cannot be placed in a single kind of octahedron without gross violation of the observed bond lengths and electron densities (Table 5). The apparent single Fe^{2+} doublet must consist of unresolved doublets due to Fe^{2+} in M(1) and M(2) of the 2:1 layer and M(3) of the interlayer sheet. Support for this interpretation comes from Mössbauer spectral studies of several Fe-bearing chlorites by Ballet *et al.* (1985) and Townsend *et al.* (1986). Both sets of authors found they could not distinguish Fe^{2+} ions in *cis* and *trans* octahedral sites of the 2:1 layer and in octahedral sites of the interlayer sheet. Townsend *et al.* (1986) attributed this lack of resolution to broadening of the Fe^{2+} magnetic-hyperfine spectrum as a result of an inhomogeneous distribution of Fe over the available octahedral sites (implying the presence of magnetic and nonmagnetic domains at certain temperatures) and random next-nearest-neighbor substitutions of other ions and vacancies (as documented in Table 5 for this specimen). The mean M–O,OH bond lengths observed in the present study confirm that the Fe present is dominantly ferrous and suggest also that the Fe^{2+}/Fe^{3+} ratio is even slightly higher than the 6.9 value given by the analysis of Clarke and Schneider (1891).

Phillips *et al.* (1980) pointed out for the triclinic II*b*-4 structure that cation-cation repulsion between the trivalent cation in interlayer site M(4) and the cations in the tetrahedral sheets immediately above and below causes offsets of the latter two sheets in opposite di-

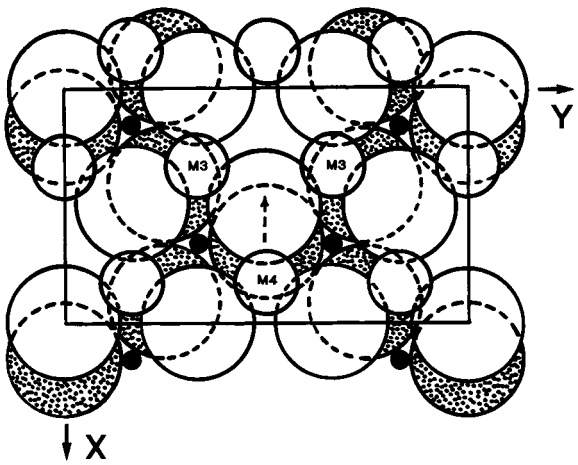

Figure 4. Lower OH plane (large open circles) of interlayer in *b* position above upper tetrahedral sheet (large stippled basal oxygens and small solid T cations) of first 2:1 layer. Small open circles are interlayer octahedral cations. Tetrahedral sheet offset parallel to dashed arrow is due to cation-cation repulsion between Al in M(4) and adjacent T cations.

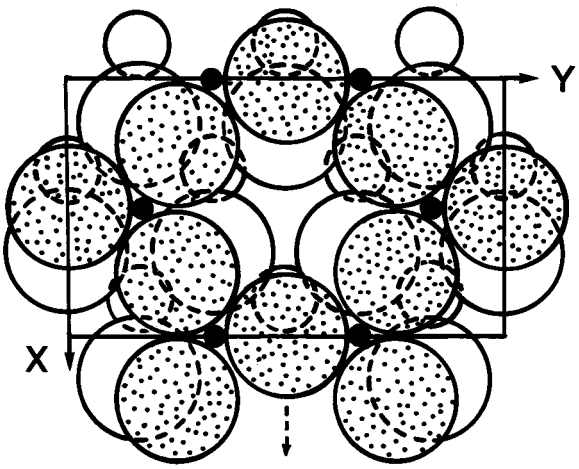

Figure 5. Basal oxygens (large stippled circles) of repeating 2:1 layer in *b* position relative to upper OH plane (large open circles) of interlayer. Dashed arrow indicates both direction of *a*/3 tetrahedral shift within lower 2:1 layer and offset of tetrahedral sheet resulting from cation-cation repulsion between Al in M(4) and adjacent T cations. Hexagonal ring of repeating layer is in "2" position.

rections. The directions of offset are diagonal to the *X* and *Y* axes along [110]; hence, that the crystallographic β angles for the two specimens are increased by 0.24° and 0.42° relative to their ideal values near 97.1°, and the crystallographic α angles are increased from 90° to 90.45° and 90.53°. The offsets provide slightly smaller T–M distances around the divalent M(3) cation for two of its four T neighbors (4.71 Å vs. 4.74–4.75 Å), than around the trivalent M(4) cation (4.74–4.75 Å), and the possibility of lessening cation-cation repulsion in this manner appears to be one of the reasons for the ordering of a trivalent cation into M(4).

For the monoclinic II*b*-2 structure, similar offsets of the tetrahedral sheets occur, but the directions of offsets are different from those in the II*b*-4 structure because of the different position of the repeating 2:1 layer (2 vs. 4). The offsets are parallel to [100] rather than [110]; hence, only the crystallographic β angle is affected. The β angle is decreased to 96.35° from its ideal value of $\beta = \text{arc cos}(-a/3c) = 97.18°$. The offsets are shown in Figures 4 and 5. Two of the four T(1)–M(3) distances are decreased (4.66 Å × 2 vs. 4.72 Å × 2) relative to the four T(1)–M(4) distances (all 4.72 Å). This means that the offsets help minimize the cation-cation repulsion resulting from localization of a trivalent element in M(4) by providing more space around M(4) at the expense of M(3). The localization is favored also by the point symmetry 2/*m* for M(4) rather than 2 for M(3). In other words, a whole Al cation can occupy site M(4), but only a hybrid $Al_{0.5}R^{2+}{}_{0.5}$ cation can occupy each of the M(3) sites on average.

The difference in offset directions of the tetrahedral sheets in the II*b*-4 and II*b*-2 structures and the successful rationalization of the offset directions as a consequence of the difference in positions of the sheets relative to the M(4) cation lend validity to the proposed explanation. Even though repulsion between cations separated by 4.7 Å cannot be large, it must be remembered that the tetrahedral sheets are constrained in position only by relatively weak interlayer bonds.

Tetrahedra

The tetrahedral Si,Al cations must be disordered in this specimen because no ordering was detected in any of the subgroup symmetries. The calculated T–O bond length of 1.670 Å for the composition of $Si_{2.622}Al_{1.378}$ is in good agreement with the observed mean bond length of 1.668 Å. Phillips *et al.* (1980) noted that a disordered Si,Al distribution gives the most favorable balance of charge around the ordered trivalent site M(4) for the II*b*-4 structure. This interpretation is consistent for any *b* position of the interlayer relative to a 2:1 layer because it places two adjacent tetrahedra equidistant from the trivalent M(4) site. Thus, neither tetrahedron is favored for concentration of Si or Al as a result of local charge balance involving ordering of the interlayer cations. Special factors may be required to promote ordering of tetrahedral cations in chlorites, as in the micas. It is believed most II*b* and I*b* (β = 90°) chlorites will have disorder of tetrahedral cations as a consequence, whereas the interlayer trivalent and divalent cations will be ordered.

The tetrahedra are rotated by 8.5° to fit better with the smaller lateral dimensions of the 2:1 octahedral sheet. Because M(1) and M(2) are so similar in size, no tilting is required of the tetrahedra to coordinate with the octahedra. The basal oxygen and interlayer

surfaces are essentially planar. The direction of rotation moves the acceptor basal oxygens closer to the donor OH groups (Figure 3) to shorten hydrogen bond contacts. These directions (in projection) also move the basal oxygens toward the positions of the 2:1 octahedral cations (which control the rotation directions completely in micas), but away from the interlayer cations (Figure 3). This is also true in the II*b*-4 structure.

Comparison of sheet and layer thicknesses

A total of five trioctahedral chlorites have now been refined by diffractometer techniques. The chlorite of this study differs from the others chemically in its high Fe content (1.755 atoms vs. 0.08–0.29 range in the others) and in its high net tetrahedral charge (−1.378 vs. −0.84 to −1.01 range). The influence of the high Fe content is manifest in a 2:1 layer that is thicker than for the other four chlorites (6.696 vs. 6.641–6.653 Å range) and an interlayer sheet that is thicker (2.024 Å) than those of the three chlorites with Mg,Al interlayers (1.976–1.995 Å range) but thinner than that of the Erzincan specimen with a Mg,Cr interlayer (2.031 Å). The high tetrahedral charge draws the interlayer much closer to the adjacent basal oxygens, however, so that the separation distance is only 2.731 Å relative to a 2.807–2.827 Å range for the other chlorites. The net result is that the d(001) value of 14.182 Å for the chlorite of this study is moderately smaller than for the others (14.238–14.332 Å range). A similarly high tetrahedral charge in an iron-poor chlorite should cause an appreciably smaller d(001) value.

Hydroxyls

The H^+ protons are located 0.9–1.0 Å from the centers of their respective oxygen host atoms. The OH(1)-H(1) vector in the 2:1 octahedral sheet makes a rho angle of 88.2° with the (001) plane. This vector points slightly toward the divalent M(1) site because the hydrogen proton is repelled from the two M(2) octahedral cations due to the trivalent Fe^{3+} content of the latter sites.

The hydrogens in the interlayer octahedral sheet form long hydrogen bonds (2.774 Å and 2.831 Å × 2) with the basal oxygens of the tetrahedral sheet. The OH(2)-H(2)-O(2) bond angle is nearly straight, but the two OH(3)-H(3)-O(3) angles are bent to 146.1°. The positions of the H^+ protons do not follow the pattern established for II*b* chlorite by Joswig *et al.* (1980) by the more accurate neutron diffraction technique, and it is considered that their positions in the present study are inaccurate.

Thermal ellipsoids

The shapes and orientations of thermal ellipsoids are presented in Table 3. All atoms have their major component of thermal vibration nearly parallel to the *Z* axis. This configuration is probably due to the fact that the crystal was so thin (0.05 mm) that the psi-scan correction for absorption was not adequate. The same effect has been noted for other refinements in this laboratory involving very thin platelets.

CONCLUSIONS

The monoclinic II*b*-2 chlorite is disordered with respect to its Si,Al tetrahedral cations. This finding is contrary to the results from the less accurate study of similar material by Steinfink (1958, 1961). The interlayer cations are ordered with trivalent Al located on a symmetry center at site M(4) and primarily divalent cations (Mg and Fe) in the two M(3) interlayer sites. A small degree of ordering of Mg, Fe^{2+}, and Fe^{3+} exists in the M(1) and M(2) octahedra within the 2:1 layer. The ratio of octahedral Fe^{2+}/Fe^{3+} cations is about 7.0 for the crystal as a whole, based on consideration of the observed octahedral bond lengths and electron densities. The excess of negative charge above unity due to tetrahedral substitution of Al for Si (1.378 atoms) is compensated within the octahedral sheet of the 2:1 layer and the remainder within the interlayer. This magnitude of the negative tetrahedral charge is about average for trioctahedral chlorites (Bailey and Brown, 1962), and the restriction of the positive interlayer charge to about +1.0 is probably the most stable arrangement.

Results to date suggest that ordering of a trivalent cation in the centrosymmetric interlayer site M(4) is universal in stable trioctahedral chlorites. Factors controlling the ordering are: (1) energy minimization by location of the source of the positive charge on the interlayer sheet in one octahedron rather than in two; this avoids disorder of divalent and trivalent interlayer cations over the M(3) sites or intermixed domainal structures; (2) lessening of cation-cation repulsion between M(4) and tetrahedral cations by tetrahedral sheet offsets; (3) higher crystal-field stabilization energy (CFSE) by location of certain trivalent transition metals, such as Cr, in the less distorted octahedron M(4); and (4) possibly local charge balance by a trivalent cation in M(4) positioned exactly between ordered Al-rich tetrahedra in the sheets immediately above and below the interlayer for *a* positions of the interlayer sheet relative to the 2:1 layers; this factor has not yet been proven. Only partial ordering of the interlayer cations was found by Joswig *et al.* (1980) for a II*b*-4 chlorite from an Alpine fissure vein. This probably is a consequence of the environment of crystallization, similar to the partial ordering found in the adularias of these veins.

Disorder of tetrahedral cations is predicted for most II*b* and I*b* ($\beta = 90°$) trioctahedral chlorites, because the *b* position of the interlayer sheet relative to the 2:1 layers above and below provides no preferential driv-

ing force for concentration of Si or Al in any tetrahedron as a consequence of the expected interlayer cation ordering. All five regular-stacking trioctahedral chlorites studied in detail to date have shown disorder of tetrahedral cations but ordering of interlayer cations.

Most chlorites have a semirandom stacking of layers and interlayers. For regular-stacking crystals the monoclinic II*b*-2 chlorite polytype is less abundant in nature than the triclinic II*b*-4 (=II*b*-6) structure. Triclinic II*b* structures result from superimposing a hexagonal ring of the repeating layer over either positions 4 or 6 of Figure 1d. A monoclinic structure results only from superposition over position 2. If the three positions are equally probable and provided no other factors control the superposition of layers, the regular-stacking triclinic structures should be twice as abundant as the monoclinic structure. In fact, however, only a few monoclinic II*b*-2 chlorites are known to the authors. It is suspected that this apparent rarity is an artifact due to the paucity of study of chlorites by single crystal X-ray methods. The observations that (1) all regularly stacked chlorite crystals from the Washington, D.C., sample are II*b*-2, and (2) the II*b*-2 polytype has not yet been identified in samples for which the II*b*-4 polytype is abundant suggest strongly that other, as yet unknown, factors also are important in determining the resultant structures. These factors may be related to the environment of crystallization.

ACKNOWLEDGMENTS

This research was supported in part by NSF grant EAR-8106124 and in part by grant 17966-AC2-C from the Petroleum Research Fund, administered by the American Chemical Society. We are indebted also to the U.S. National Museum for provision of the sample studied, Michael Brauner for the microprobe analysis, and Lisa Heller-Kallai for information about an earlier Mössbauer study of material from the same locality.

REFERENCES

Bailey, S. W. (1972) Determination of chlorite compositions by X-ray spacings and intensities: *Clays & Clay Minerals* **20,** 381–388.

Bailey, S. W. (1986) Re-evaluation of ordering and local charge-balance in I*a* chlorite: *Canadian Mineral.* **24,** 649–654.

Bailey, S. W. and Brown, B. E. (1962) Chlorite polytypism: I. Regular and semi-random one-layer structures: *Amer. Mineral.* **47,** 819–850.

Ballet, O., Coey, J. M. D., and Burke, K. J. (1985) Magnetic properties of sheet silicates; 2:1:1 layer minerals: *Phys. Chem. Minerals* **12,** 370–378.

Bish, D. L. and Giese, R. F., Jr. (1981) Interlayer bonding in IIb chlorite: *Amer. Mineral.* **66,** 1216–1220.

Brown, B. E. and Bailey, S. W. (1963) Chlorite polytypism: II. Crystal structure of a one-layer Cr-chlorite: *Amer. Mineral.* **48,** 42–61.

Busing, W. R., Martin, K. O., and Levy, H. A. (1962) ORFLS, a Fortran crystallographic least-squares refinement program: *Oak Ridge National Laboratory Tech. Manual* **305,** 75 pp.

Busing, W. R., Martin, K. O., and Levy, H. A. (1964) ORFFE, a Fortran crystallographic function and error program: *Oak Ridge National Laboratory Tech. Manual* **306,** 83 pp.

Clarke, F. W. and Schneider, E. A. (1891) Experiments upon the constitution of the natural silicates: *U.S. Geol. Surv. Bull.* **78,** 11–33.

Cromer, D. T. and Mann, J. B. (1968) X-ray scattering factors computed from numerical Hartree-Fock wave functions: *Acta Crystallogr.* **A24,** 321–324.

Dollase, W. A. (1980) Optimum distance model of relaxation around substitutional defects: *Phys. Chem. Minerals* **6,** 255–304.

Joswig, W., Fuess, H., Rothbauer, R., Takéuchi, Y., and Mason, S. A. (1980) A neutron diffraction study of a one-layer triclinic chlorite: *Amer. Mineral.* **65,** 349–352.

Lister, J. S. and Bailey, S. W. (1967) Chlorite polytypism: IV. Regular two-layer structures: *Amer. Mineral.* **52,** 1614–1631.

North, A. C. T., Philips, D. C., and Mathews, F. (1968) A semi-empirical method of absorption correction: *Acta Crystallogr.* **A24,** 351–359.

Phillips, T. L., Loveless, J. K., and Bailey, S. W. (1980) Cr^{3+} coordination in chlorites: A structural study of ten chromian chlorites: *Amer. Mineral.* **65,** 112–122.

Steinfink, H. (1958) The crystal structure of chlorite. I. A monoclinic polymorph: *Acta Crystallogr.* **11,** 195–198.

Steinfink, H. (1961) Accuracy in structure analysis of layer silicates: Some further comments on the structure of prochlorite: *Acta Crystallogr.* **14,** 198–199.

Townsend, M. G., Longworth, G., and Kodama, H. (1986) Magnetic interaction at low temperature in chlorite and its products of oxidation: A Mössbauer investigation: *Can. Mineral.* **24,** 105–115.

Weiss, Z., Rieder, M., Chmielová, M., and Krajíček, J. (1985) Geometry of the octahedral coordination in micas: A review of refined structures: *Amer. Mineral.* **70,** 747–757.

(Received 7 June 1986; accepted 8 October 1986; Ms. 1596)